

Finite-temperature behavior of the Bose polaron

Jesper Levinsen and Meera M. Parish

School of Physics and Astronomy, Monash University, Victoria 3800, Australia

Rasmus S. Christensen, Jan J. Arlt, and Georg M. Bruun

Department of Physics and Astronomy, Aarhus University, DK-8000 Aarhus C, Denmark.

(Dated: January 1, 2018)

We consider a mobile impurity immersed in a Bose gas at finite temperature. Using perturbation theory valid for weak coupling between the impurity and the bosons, we derive analytical results for the energy and damping of the impurity for low and high temperatures, as well as for temperatures close to the critical temperature T_c for Bose-Einstein condensation. These results show that the properties of the impurity vary strongly with temperature. In particular, the energy exhibits a non-monotonic behavior close to T_c , and the damping rises sharply close to T_c . We argue that this behaviour is generic for impurities immersed in an environment undergoing a phase transition that breaks a continuous symmetry. Finally, we discuss how these effects can be detected experimentally.

I. INTRODUCTION

The experimental realization of highly population-imbalanced atomic gases has dramatically improved our understanding of the properties of mobile impurities in a quantum medium. Using Feshbach resonances [1] to tune the interaction between the impurity and the reservoir, cold-atom experiments have systematically explored the properties of impurities first in fermionic [2–4] and recently also in bosonic [5, 6] reservoirs. While there are many similarities between impurities in fermionic and bosonic reservoirs (termed the Fermi and Bose polaron, respectively), there are also important differences. For instance, whereas the Fermi polaron has a sharp transition to a molecular state with increasing attraction [7–15], the Bose polaron exhibits a smooth crossover instead, either to a molecular state [16] or the lowest Efimov trimer [17] depending on the value of the three-body parameter. The Bose polaron has also been proposed to be unstable towards other lower lying states [18, 19].

Here, we investigate a unique feature of the Bose polaron (polaron from now on): The medium exhibits a phase transition between a Bose-Einstein condensate (BEC) and a normal gas. The effect of such a transition on the quasiparticle properties has not been explored before in previous finite-temperature studies of the Bose polaron [20, 21]. Using perturbation theory valid for weak coupling, we show that this transition gives rise to several interesting effects. Both the energy and the damping of the polaron depend strongly and in a non-trivial way on the temperature in the region around the critical temperature T_c . More generally, these effects are relevant to the behavior of quasiparticles near a phase transition that breaks a continuous symmetry of the system. We discuss how these effects can be measured. Very recently, the temperature dependence of the polaron was investigated for strong coupling [22]. Our present study focuses instead on the weak-coupling regime where rigorous results can be derived.

The paper is organized as follows. In Sec. II we de-

scribe the model and introduce the perturbative framework. Our main results are presented in Sec. III. Here we describe the polaron properties in three different temperature regimes: at low temperature, in the region close to the critical temperature for Bose-Einstein condensation, and all the way to high temperature. We conclude in Sec. IV.

II. MODEL AND METHODS

We consider an impurity of mass m in a gas of bosons with mass m_B . The Hamiltonian is

$$H = \sum_{\mathbf{k}} \epsilon_{\mathbf{k}}^B b_{\mathbf{k}}^\dagger b_{\mathbf{k}} + \frac{g_B}{2} \sum_{\mathbf{k}, \mathbf{k}', \mathbf{q}} b_{\mathbf{k}+\mathbf{q}}^\dagger b_{\mathbf{k}'-\mathbf{q}}^\dagger b_{\mathbf{k}'} b_{\mathbf{k}} + \sum_{\mathbf{k}} \epsilon_{\mathbf{k}} c_{\mathbf{k}}^\dagger c_{\mathbf{k}} + g \sum_{\mathbf{k}, \mathbf{k}', \mathbf{q}} c_{\mathbf{k}+\mathbf{q}}^\dagger b_{\mathbf{k}'-\mathbf{q}}^\dagger b_{\mathbf{k}'} c_{\mathbf{k}}, \quad (1)$$

where the operators $b_{\mathbf{k}}^\dagger$ and $c_{\mathbf{k}}^\dagger$ create a boson and the impurity, respectively, with momentum \mathbf{k} and free dispersions $\epsilon_{\mathbf{k}}^B = k^2/2m_B$ and $\epsilon_{\mathbf{k}} = k^2/2m$. The boson-boson and the boson-impurity interactions are short range with coupling strengths g_B and g , respectively, and we work in units where the volume, \hbar , and k_B are 1.

The Bose gas is taken to be weakly interacting, i.e., $na_B^3 \ll 1$, where n is the boson density and $a_B > 0$ is the boson-boson scattering length. As we are interested in deriving rigorous results, we use Popov theory to describe the Bose gas. Below the BEC critical temperature $T_c \simeq \frac{2\pi}{[\zeta(3/2)]^{2/3}} \frac{n^{2/3}}{m_B}$, we have the usual Bogoliubov dispersion $E_{\mathbf{k}} = [\epsilon_{\mathbf{k}}^B(\epsilon_{\mathbf{k}}^B + 2\mathcal{T}_B n_0)]^{1/2}$, where n_0 is the condensate density, and $\mathcal{T}_B = 4\pi a_B/m_B$ the boson vacuum scattering matrix. Below T_c , we have the normal and anomalous propagators for the bosons in the BEC,

$$G_{11}(\mathbf{k}, i\omega_s) = \frac{u_{\mathbf{k}}^2}{i\omega_s - E_{\mathbf{k}}} - \frac{v_{\mathbf{k}}^2}{i\omega_s + E_{\mathbf{k}}} \\ G_{12}(\mathbf{k}, i\omega_s) = G_{21}(\mathbf{k}, i\omega_s) = \frac{u_{\mathbf{k}} v_{\mathbf{k}}}{i\omega_s + E_{\mathbf{k}}} - \frac{u_{\mathbf{k}} v_{\mathbf{k}}}{i\omega_s - E_{\mathbf{k}}}. \quad (2)$$

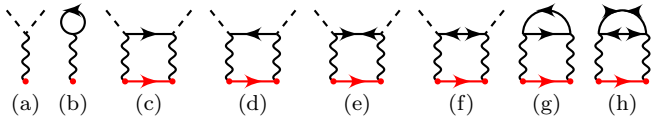


FIG. 1: (a-b) First and (c-h) second order diagrams for the impurity self-energy. The impurity propagator is shown as the bottom red lines, and the external impurity propagators attach to the red dots. The boson normal and anomalous propagators are shown as the upper solid black lines, while dashed lines are condensed bosons. The wavy vertical lines denote the impurity-boson scattering matrix \mathcal{T}_v .

where $u_{\mathbf{k}}^2 = 1 + v_{\mathbf{k}}^2 = [(\epsilon_{\mathbf{k}}^B + \mathcal{T}_B n_0)/E_{\mathbf{k}} + 1]/2$ are the coherence factors, and $\omega_s = i2sT$ is a boson Matsubara frequency with s integer. The condensate density is then found self-consistently from the condition

$$\begin{aligned} n &= n_0 - T \sum_{\omega_s, \mathbf{k}} e^{i\omega_s 0^+} G_{11}(\mathbf{k}, i\omega_s) \\ &= n_0 + \frac{8n_0}{3\sqrt{\pi}} (n_0 a_B^3)^{1/2} + \sum_{\mathbf{k}} \frac{\epsilon_{\mathbf{k}}^B + \mathcal{T}_B n_0}{E_{\mathbf{k}}} f_{\mathbf{k}}. \end{aligned} \quad (3)$$

where $f_{\mathbf{k}} = [\exp(E_{\mathbf{k}}/T) - 1]^{-1}$ is the Bose distribution function for temperatures $T < T_c$. Popov theory provides an accurate description except in a narrow critical region determined by $|T - T_c|/T_c \lesssim n^{1/3} a_B$ [23].

A. Perturbation theory

We use perturbation theory in powers of the impurity-boson scattering length a to analyze the impurity problem. At $T = 0$, this approach has yielded important information. For instance, the impurity energy was shown to depend logarithmically on a at third order [24], similarly to the energy of a weakly interacting Bose gas beyond Lee, Huang, and Yang [25, 26]. The first order self-energy in Fig. 1(a,b) gives the mean-field energy shift $\Sigma_1 = \mathcal{T}_v n$, where $\mathcal{T}_v = 2\pi a/m_r$ is the boson-impurity scattering amplitude at zero energy, with $m_r = m_B m/(m_B + m)$ the reduced mass. This shift is independent of temperature, and in order to get a non-trivial T -dependence, we need to go to second order.

The six possible second order diagrams are shown in Fig. 1. Diagrams (c-f) yield the ‘‘Frohlich’’ contribution

$$\begin{aligned} \Sigma_2^F(\mathbf{p}, \omega) &= n_0(T) \mathcal{T}_v^2 \sum_{\mathbf{k}} \left[\frac{1}{\epsilon_{\mathbf{k}}^B + \epsilon_{\mathbf{k}}^B} \right. \\ &\quad \left. + \frac{\epsilon_{\mathbf{k}}^B}{E_{\mathbf{k}}} \left(\frac{1 + f_{\mathbf{k}}}{\omega - E_{\mathbf{k}} - \epsilon_{\mathbf{k}+\mathbf{p}}} + \frac{f_{\mathbf{k}}}{\omega + E_{\mathbf{k}} - \epsilon_{\mathbf{k}+\mathbf{p}}} \right) \right], \end{aligned} \quad (4)$$

where the frequency ω is taken to have an infinitesimal positive imaginary part. The first term in the integrand comes from replacing the bare boson-impurity interaction g with the scattering matrix \mathcal{T}_v (see, e.g., Ref. [24]). These diagrams are non-zero only for $T \leq T_c$, as they

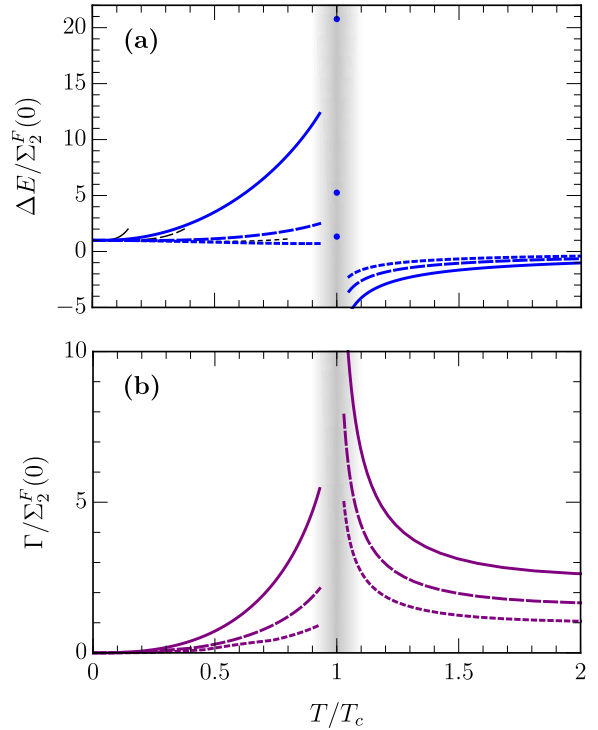


FIG. 2: (a) Second order energy shift and (b) decay rate for $m = m_B$. The lines are for $n^{1/3} a_B$ taking the values 0.04 (solid), 0.1 (dashed), and 0.25 (short dashed). In (a) we also show the $T = T_c^-$ prediction (12) for the three interaction values (dots), as well as the low-temperature prediction to fourth order in T/T_c (thin, black). The shaded region illustrates where Popov theory is expected to fail.

correspond to the scattering of a boson into or out of the condensate. The term Σ_2^F can also be obtained from the Frohlich model [27–29].

The ‘‘bubble’’ diagrams (g-h) of Fig. 1 give

$$\begin{aligned} \Sigma_2^B(\mathbf{p}, \omega) &= \mathcal{T}_v^2 \sum_{\mathbf{k}} [v_{\mathbf{k}}^2 (1 + f_{\mathbf{k}}) \Pi_{11}(\mathbf{k} + \mathbf{p}, \omega - E_{\mathbf{k}}) \\ &\quad - u_{\mathbf{k}} v_{\mathbf{k}} [(1 + f_{\mathbf{k}}) \Pi_{12}(\mathbf{k} + \mathbf{p}, \omega - E_{\mathbf{k}}) + \\ &\quad f_{\mathbf{k}} \Pi_{12}(\mathbf{k} + \mathbf{p}, \omega + E_{\mathbf{k}})] + u_{\mathbf{k}}^2 f_{\mathbf{k}} \Pi_{11}(\mathbf{k} + \mathbf{p}, \omega + E_{\mathbf{k}})] \end{aligned} \quad (5)$$

where the pair propagators Π_{11} and Π_{12} are given in Appendix A. The bubble diagrams have not previously been evaluated, as they require particles excited out of the condensate and consequently are suppressed by a factor $\sqrt{n_0 a_B^3}$ for $T \ll T_c$ compared with the Frohlich diagrams. Their magnitude, however, increases with T as particles get thermally excited out of the BEC, and Σ_2^B is indeed the only non-zero contribution to second order for $T > T_c$. Note that the Frohlich model does not include Σ_2^B and therefore cannot describe the polaron correctly for finite T [24].

III. BOSE POLARON AT FINITE TEMPERATURE

The polaron energy $E_{\mathbf{p}}$ for a given momentum \mathbf{p} is found by solving $E_{\mathbf{p}} = \epsilon_{\mathbf{p}} + \text{Re}[\Sigma(\mathbf{p}, E_{\mathbf{p}})]$. Here, we focus on an impurity with momentum $\mathbf{p} = \mathbf{0}$. To second order in a , it is sufficient to evaluate the self-energy for zero frequency [24], and the equation for the polaron energy therefore simplifies to

$$E = \text{Re}[\Sigma(\mathbf{0}, 0)] = \mathcal{T}_v n + \text{Re}[\Sigma_2^F(\mathbf{0}, 0) + \Sigma_2^B(\mathbf{0}, 0)]. \quad (6)$$

The broadening of the polaron is given by $\Gamma = -\text{Im}[\Sigma_2^F(\mathbf{0}, 0) + \Sigma_2^B(\mathbf{0}, 0)]$. To simplify the notation, we will suppress the momentum and energy arguments of the self-energy, as these are zero. Instead, we will write $\Sigma(T)$ to focus on the T -dependence.

Our main results for the second-order polaron energy shift, $\Delta E \equiv E - \mathcal{T}_v n$, and broadening Γ are shown in Fig. 2 for $m = m_B$. We observe a strong temperature dependence, along with an intriguing non-monotonic behavior across the phase transition. We discuss the various regimes and limiting cases in the following. For concreteness, we mainly discuss the case of equal masses $m_B = m$, with the equations for $m_B \neq m$ relegated to the appendices.

A. Low-temperature behavior

The term $\Sigma_2^F(T)$ can be evaluated analytically for $T = 0$, giving [24, 28, 29]

$$\Sigma_2^F(0) = \frac{32\sqrt{2}}{3} \frac{a^2 n_0}{m\xi_0}, \quad (7)$$

where ξ_0 is the healing length $\xi = 1/\sqrt{8\pi n_0 a_B}$ evaluated at zero temperature. An analytic expression for general mass ratio is given in Ref. [28].

When evaluating Σ_2^B , we find that it contains terms that diverge logarithmically at large momentum. This is similar to the third order logarithmic divergence in the polaron energy at $T = 0$ [24]. The divergence can be cured by including the momentum dependence of the scattering matrix, which provides an ultraviolet cut-off at the scale $1/k = a^* \sim \max(a, a_B)$. Since the healing length sets the lower limit in the momentum integral, we find

$$\Sigma_2^B(0) \simeq \frac{4\sqrt{6\pi} a^2 n_0}{m\xi_0} \left(\frac{2\pi}{3\sqrt{3}} - 1 \right) \sqrt{n_0 a_B^3} \ln(a^*/\xi), \quad (8)$$

where we ignore terms of order $(n_0 a a_B)^2$. Equation (8) is suppressed by $(n_0 a_B^3)^{1/2}$ compared with $\Sigma_2^F(0)$, and we thus ignore the terms in Σ_2^B that give rise to this divergence and focus on the remainder, denoted $\tilde{\Sigma}_2^B(T)$ (see Appendix B for details). Note that a divergent term of the form (8) in the self-energy is to be expected, since

at $a = a_B$ the polaron ground state energy must correspond to the chemical potential of a weakly interacting Bose gas, i.e., $E = \partial E_{\text{WS}}/\partial n$, with E_{WS} the energy of the weakly interacting Bose gas including the correction by Wu and Sawada [25, 26]. From this argument, we also conclude that there must be a similar contribution arising from the Fröhlich type diagrams if we treat the excitations of the BEC beyond Bogoliubov theory. Such an investigation is beyond the scope of this work.

To proceed, we take advantage of how the self-energy below T_c simplifies into a product of a T -dependent prefactor and a function of ξ/λ , where $\lambda = (2\pi/m_B T)^{1/2}$ is the de Broglie wavelength. Specifically

$$\Sigma_2^F(T) = \Sigma_2^F(0) \left(\frac{n_0(T)}{n_0(0)} \right)^{3/2} [1 + \mathcal{I}_F(\xi/\lambda)]. \quad (9)$$

Here \mathcal{I}_F is a dimensionless form of the integral appearing in (4), see Appendix B for details. It vanishes at $T = 0$ and its imaginary part at low temperature is only non-zero when $m < m_B$ (Appendix C). Similarly to Eq. (9), an expression for $\tilde{\Sigma}_2^B(T)$ which explicitly contains the additional suppression factor $(n_0 a_B^3)^{1/2}$ is given in Appendix B.

Due to the suppression factor, at low temperature we neglect $\tilde{\Sigma}_2^B$ and focus on Σ_2^F . Here, the superfluid density $n_0(T)$ decreases as T^2 for $T \ll T_c$ [23, 30], which from Eq. (9) gives a T^2 decrease in the polaron energy. Indeed, expanding Eq. (3) at low temperature yields

$$\frac{n - n_0(T)}{n} \simeq \frac{\pi^{3/2} (T/T_c)^2}{6\zeta(\frac{3}{2})^{4/3} (na_B^3)^{1/6}} - \frac{\pi^{7/2} (T/T_c)^4}{480\zeta(\frac{3}{2})^{8/3} (na_B^3)^{5/6}}, \quad (10)$$

where at each order in T/T_c we keep only the leading order contribution in na_B^3 . However, we find that $\mathcal{I}_F(\xi/\lambda) \propto (na_B^3)^{-4/3} (T/T_c)^4$ for $T \ll T_c$, and since this increase is proportional to $(na_B^3)^{-4/3}$, it quickly dominates for a weakly interacting BEC. As a result, we obtain

$$E(T) \simeq E(0) + \frac{\pi^2 a^2 T^4}{60 a_B^2 n c^3}, \quad (11)$$

where we have introduced the speed of sound in the BEC: $c = (4\pi a_B n)^{1/2}/m$. Interestingly, the low T dependence of the polaron energy (11) can be related to the free energy of phonons in a weakly interacting BEC for $T \ll T_c$: $F_{\text{ph}} = -\pi^2 T^4/(90c^3)$ [31]. Indeed, setting $a = a_B$ we find that (11) exactly matches the change in the BEC chemical potential due to the thermal excitation of phonons, i.e. $\Delta\mu = -\partial F_{\text{ph}}/\partial n|_{T,V}$. To our knowledge, this T^4 increase in the chemical potential of a weakly interacting BEC has never been measured. Our result thus suggests a way to measure this effect using for instance radio-frequency (RF) spectroscopy on the impurity [5, 6].

B. Behavior close to T_c

We now turn our attention to temperatures close to T_c . From Eq. (4) it follows that $\Sigma_2^F(T) \propto n_0(T)$ and one would at first sight expect that it vanishes as $T \rightarrow T_c^-$. This is in fact *not* the case when $m = m_B$. Expanding Eq. (4) to lowest order in n_0 yields

$$\Sigma_2^F(T_c^-) = \frac{\mathcal{T}_v^2}{\mathcal{T}_B} \sum_{\mathbf{k}} f_{\mathbf{k}} = 4\pi \frac{na^2}{ma_B}. \quad (12)$$

Thus, $\Sigma_2^F(T)$ has a *non-zero* value $\propto 1/a_B$ when $T \rightarrow T_c^-$. Since Σ_2^F obviously is zero for $T > T_c$, this means that it is *discontinuous* at T_c . The origin of this surprising result is that the low energy spectrum of the Bose gas changes from linear to quadratic in momentum at T_c , increasing the density-of-states dramatically. Consequently, the diagram given by Fig. 1(d), describing the scattering of the impurity on a thermally excited boson, develops an infrared divergence for $n_0 \rightarrow 0$ when $m = m_B$. For $m \neq m_B$, we on the other hand find $\Sigma_2^F(T_c^-) = 0$ so that Σ_2^F is continuous across T_c , see Appendix B.

Above T_c , $\tilde{\Sigma}_2^B(T)$ is the only non-zero second-order term and Eq. (5) simplifies considerably since $v_{\mathbf{k}} = 0$ and $E_{\mathbf{k}}$ becomes $\epsilon_{\mathbf{k}}^B + \mathcal{T}_B n - \mu$; i.e. Popov theory corresponds to the Hartree-Fock approximation for $T > T_c$. The boson chemical potential is therefore $\mu = \mu_{\text{id}} + \mathcal{T}_B n$, with μ_{id} the chemical potential of an ideal Bose gas. We obtain

$$\frac{\Sigma_2(T > T_c)}{\Sigma_2^F(T = 0)} = -\frac{1}{\sqrt{n_0^{1/3}(0)a_B}} \left[\mathcal{I}_N(T/T_c) + i \frac{3\sqrt{\pi}[\text{Li}_2(z) + \frac{1}{2} \log^2(1-z)]}{16\zeta^{4/3}(3/2)} \left(\frac{T}{T_c} \right)^2 \right], \quad (13)$$

where we have used the ideal Bose gas relation $n\lambda^3 = \text{Li}_{3/2}(z)$, with Li the polylogarithm and $z \equiv \exp(\mu_{\text{id}}/T)$ the fugacity. The dimensionless function $\mathcal{I}_N(T/T_c)$ is given in Appendix D. It follows from Eq. (13) that the imaginary part of the self-energy diverges as $\log^2(1-z)$ when $z \rightarrow 1$ for $T \rightarrow T_c^+$. This comes from infrared divergences in the integrals containing the Bose distribution function. Physically, it means that the polaron becomes strongly damped close to T_c . The real part of $\Sigma_2(T)$ can also be shown to diverge when $T \rightarrow T_c^+$ as outlined in Appendix D.

C. High-temperature behavior

Finally, we consider the limit $T \gg T_c$. Expanding the self-energy to lowest order in the fugacity z yields

$$\frac{\Sigma_2^B(T)}{\Sigma_2^F(0)} \simeq -\kappa \left[0.315 \frac{T_c}{T} + i \frac{3\sqrt{\pi}}{16\zeta(3/2)^{1/3}} \sqrt{\frac{T}{T_c}} \right] \quad (14)$$

with $\kappa = [n_0(0)a_B^3]^{-1/6}$. Thus, whereas the energy shift of the polaron decreases with increasing temperature, the

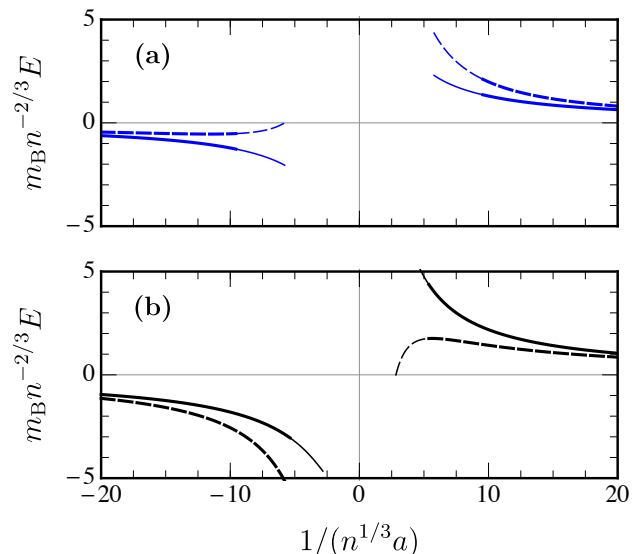


FIG. 3: Polaron energy as a function of interaction strength. (a) $m = m_B$ and $n^{1/3} a_B = 0.003$ as in the Aarhus experiment [5] for $T = 0$ (solid line) and $T = T_c/10$ (dashed). (b) $m/m_B = 40/87$ and $n^{1/3} a_B = 0.03$ as in the JILA experiment [6] with $T = 0$ (solid line) and $T = T_c/2$ (dashed). The lines are thinner in the regime $a^2 > a_B \xi_0$ where the polaron ceases to be a well-defined quasiparticle [24], and they are only plotted in the range where the finite-temperature 2nd order shift is smaller than the mean-field energy. Note that our perturbative results are reliable at a higher temperature in the JILA experiment since the gas parameter $n^{1/3} a_B$ is larger than in the Aarhus experiment.

polaron becomes increasingly damped as the impurity collides with more and more energetic bosons.

D. Validity of perturbation theory

At $T = 0$, the small parameter of perturbation theory is a/ξ and we additionally require $a^2/a_B \xi \ll 1$ for the polaron to be well-defined [24]. In general, we expect perturbation theory to be valid provided $\Sigma_2 < \Sigma_1$. From this, we derive the condition $|a| \ll a_B$ valid close to T_c , by comparing (12) with the first order shift $\mathcal{T}_v n$. For a small gas parameter, $n^{1/3} a_B$, this condition is much stricter than the $T = 0$ conditions. We therefore expect perturbation theory to break down earlier for temperatures close to T_c . Above T_c , perturbation theory is accurate when $n^{-1/3} \lambda \gg |a|$. Note also that perturbation theory breaks down in the critical region $|T - T_c|/T_c \lesssim n^{1/3} a_B$ [23, 32], which is the origin of the infrared divergences as $T \rightarrow T_c$. However, the critical region is narrow for a weakly interacting BEC, making our results reliable except very close to T_c .

E. Numerical results

In Fig. 2, we plot the second-order self-energy Σ_2 as a function of T , evaluated numerically using Eq. (9) for various values of the gas parameter. We see an intriguing non-monotonic temperature dependence of both the polaron energy shift and damping. For $T < T_c$, the energy shift increases and the numerical results recover our predicted T^4 behavior in Eq. (11) for $T \ll T_c$. In particular, the rate of the increase scales with $a_B^{-7/2}$ so that there is a strong temperature dependence when the gas parameter of the BEC is small. The damping of the polaron, $\Gamma = -\text{Im}\Sigma_2$, also increases with T as more thermally excited bosons scatter on the impurity. Both the energy shift and the damping vary strongly close to T_c . This reflects both the logarithmic divergences discussed above as well as the discontinuous jump in the Fröhlich self-energy at T_c given by Eq. (12), which is indicated by \bullet 's in Fig. 2. Since perturbation theory breaks down close to T_c , we do not plot the numerical results in this region. For $T > T_c$, the energy shift of the polaron decreases and it vanishes as $T \rightarrow \infty$. The predicted increase in the damping rate for $T \gg T_c$ in Eq. (14) is not visible in the range of temperatures shown in Fig. 2 which focuses on the phase transition region.

In Fig. 3, we plot the total polaron energy $\Sigma_1 + \Sigma_2$ as a function of the interaction parameter $1/n^{1/3}a$ for zero and finite temperature. We consider both the Aarhus ^{39}K experiment and the JILA ^{40}K - ^{87}Rb experiment, where the latter corresponds to the case of a light impurity. In the region where we expect perturbation theory to be reliable, we see that the polaron energy for the equal-mass Aarhus case is shifted significantly higher by temperature, even when $T \ll T_c$. Moreover, we find a small decay rate $\Gamma \ll \Delta E$ in this regime. Thus, the polaron energy shift should be measurable, as we discuss below. On the other hand, the light impurity in the JILA case has a finite-temperature energy shift that is negative rather than positive. The reason is that — contrary to the equal mass case — $\Sigma_2^F(T)$ is now continuous across T_c where it goes to zero, as discussed in Sec. III B. Its positive contribution to the polaron energy is therefore much smaller, and the overall temperature shift becomes negative. The decay rate Γ on the other hand, is comparable to $|\Delta E|$ in the regime where $|\Delta E|$ is significant for the JILA parameters. This can be traced to the fact that $\Sigma_2^F(T)$ develops a pole and corresponding imaginary part when $m < m_B$ — see Appendix C for an analytic expression for $\text{Im}\Sigma_2^F$. Physically the pole originates from processes where thermally excited Bogoliubov modes scatter resonantly on the polaron. These scattering are possible since the equation $\epsilon_{\mathbf{k}} = E_{\mathbf{k}}$ has a solution for $m < m_B$, and they lead to decay.

IV. DISCUSSION AND CONCLUSION

The non-trivial temperature dependence of the impurity properties close to T_c is due to quite generic physics and is not limited to the specific system at hand. It originates from the change of the dispersion from quadratic to linear at T_c , which is a consequence of the $U(1)$ symmetry breaking resulting from the formation of a condensate. This dramatically changes the low-energy density of states of the Bose gas, which impacts the excitations that couple strongly to the impurity. Thus, similar effects should occur in other systems involving impurities coupled to a reservoir that undergoes a phase transition where a continuous symmetry is broken. This includes impurities in helium mixtures [33], conventional or high T_c superconductors [34], magnetic systems [35], and nuclear matter [36].

The temperature dependence of the polaron energy can be investigated by RF spectroscopy of ^{39}K atoms. In these experiments, a RF pulse transfers a small fraction of atoms from a BEC in the $|F = 1, m_F = -1\rangle$ state into the $|1, 0\rangle$ state, such that they form mobile impurities. The impurity-BEC interaction is highly tunable using a Feshbach resonance and thus the polaron energy can be obtained both for attractive and repulsive interactions. As shown in Fig. 3, the energy shift due to a finite temperature is sizable in the regime where perturbation theory should be reasonable: at $1/(n^{1/3}a) = 10$ the energy at $T = T_c/10$ compared to $T = 0$ corresponds to a RF frequency shift of ~ 7 kHz, which is comparable to the experimental resolution. Since the temperature dependence of the polaron energy scales with $\Sigma_2^F(0) \propto a^2 n_0$, it is favorable to access a given interaction strength by choosing a large scattering length and accordingly small density.

To conclude, using perturbation theory valid in the weak coupling regime, we investigated the properties of the Bose polaron as a function of temperature. We derived analytical results both for low temperature $T \ll T_c$, $T \simeq T_c$, and high temperature $T \gg T_c$. These results show that the superfluid phase transition of the surrounding Bose gas has strong effects on the properties of the polaron. The energy depends in a non-trivial way on T with a pronounced non-monotonic behaviour around T_c , and the damping increases sharply as T_c is approached. We argued that these effects should occur in a wide range of systems consisting of impurities immersed in an environment undergoing a phase transition. Finally, we discussed how this intriguing temperature dependence can be detected experimentally.

Acknowledgments

We thank M. W. Zwierlein for pointing out the interesting analogy between Eq. (11) and the energy of a phonon gas in a BEC. We appreciate useful discussions with B. Zhu. JL, MMP, and GMB acknowledge finan-

cial support from the Australian Research Council via Discovery Project No. DP160102739. JL is supported through the Australian Research Council Future Fellowship FT160100244. JL and MMP acknowledge funding from the Universities Australia – Germany Joint Research Co-operation Scheme. GMB wishes to acknowl-

edge the support of the Villum Foundation via grant VKR023163. JA acknowledges support from the Danish Council for Independent Research and the Villum Foundation. This work was performed in part at the Aspen Center for Physics, which is supported by the National Science Foundation Grant No. PHY-1607611.

Appendix A: Pair propagators

After performing the Matsubara frequency sums, we obtain

$$\Pi_{11}(p) = \sum_{\mathbf{k}} \left[\frac{u_{\mathbf{k}}^2(1+f_{\mathbf{k}})}{z - E_{\mathbf{k}} - \epsilon_{\mathbf{k}+\mathbf{p}}} + \frac{v_{\mathbf{k}}^2 f_{\mathbf{k}}}{z + E_{\mathbf{k}} - \epsilon_{\mathbf{k}+\mathbf{p}}} + \frac{2m_r}{k^2} \right] \quad (\text{A1})$$

for the normal pair propagator at four-momentum $p = (\mathbf{p}, z)$, and

$$\Pi_{12}(p) = -T \sum_{\omega_\nu} G_{12}(-\mathbf{k}, -\omega_\nu) G(\mathbf{k} + \mathbf{p}, \omega_\nu + z) = \sum_{\mathbf{k}} \left[\frac{u_{\mathbf{k}} v_{\mathbf{k}} (1+f_{\mathbf{k}})}{E_{\mathbf{k}} + \epsilon_{\mathbf{k}+\mathbf{p}} - z} + \frac{u_{\mathbf{k}} v_{\mathbf{k}} f_{\mathbf{k}}}{\epsilon_{\mathbf{k}+\mathbf{p}} - E_{\mathbf{k}} - z} \right], \quad (\text{A2})$$

$$\Pi_{22}(p) = -T \sum_{\omega_\nu} G_{22}(-\mathbf{k}, -\omega_\nu) G(\mathbf{k} + \mathbf{p}, \omega_\nu + z) = \sum_{\mathbf{k}} \left[\frac{u_{\mathbf{k}}^2 f_{\mathbf{k}}}{z + E_{\mathbf{k}} - \epsilon_{\mathbf{k}+\mathbf{p}}} + \frac{v_{\mathbf{k}}^2 (1+f_{\mathbf{k}})}{z - E_{\mathbf{k}} - \epsilon_{\mathbf{k}+\mathbf{p}}} \right] \quad (\text{A3})$$

for the anomalous and particle-hole propagators.

Appendix B: Self-energy below T_c : Fröhlich and bubble diagram integrals

To find the polaron energy within perturbation theory, we evaluate the Fröhlich diagrams at zero momentum and frequency, but finite temperature:

$$\begin{aligned} \Sigma_2^F(T) &= n_0(T) \mathcal{T}_v^2 \sum_{\mathbf{k}} \left[\frac{1}{\epsilon_{\mathbf{k}} + \epsilon_{\mathbf{k}}^B} + \frac{\epsilon_{\mathbf{k}}^B}{E_{\mathbf{k}}} \left(\frac{1+f_{\mathbf{k}}}{-E_{\mathbf{k}} - \epsilon_{\mathbf{k}}} + \frac{f_{\mathbf{k}}}{E_{\mathbf{k}} - \epsilon_{\mathbf{k}}} \right) \right] \\ &= \underbrace{\frac{2\pi n_0(0) a^2}{m_r \xi_0} A(\alpha)}_{\Sigma_2^F(T=0)} \left(\frac{n_0(T)}{n_0(0)} \right)^{3/2} \left[1 + \underbrace{\frac{2}{\pi} \frac{1+1/\alpha}{A(\alpha)} \int \bar{f}_{\mathbf{k}} \frac{k^2 dk}{\sqrt{k^2+2}} \left(\frac{-1}{\sqrt{k^2+2} + k/\alpha} + \frac{1}{\sqrt{k^2+2} - k/\alpha} \right)}_{\mathcal{I}_F(\xi/\lambda, \alpha)} \right], \quad (\text{B1}) \end{aligned}$$

where we have switched to dimensionless variables in the second line, measuring momentum in units of the inverse healing length. Here $\alpha \equiv m/m_B$ is the mass ratio and ξ_0 is the BEC healing length evaluated at $T = 0$. The Bose distribution in dimensionless units is

$$\bar{f}_{\mathbf{k}} = \frac{1}{\exp \left[\frac{\lambda^2}{4\pi\xi_0^2} k \sqrt{k^2+2} \right] - 1}. \quad (\text{B2})$$

The function defined in the main text for equal masses is $\mathcal{I}_F(\xi/\lambda) \equiv \mathcal{I}_F(\xi/\lambda, 1)$. For $T \ll T_c$ we have

$$\mathcal{I}_F(\xi/\lambda) \simeq \frac{\pi^4}{1280 \zeta(\frac{3}{2})^{8/3} (na_B^3)^{4/3}} \left(\frac{T}{T_c} \right)^4. \quad (\text{B3})$$

The mass-ratio dependent function A was found for general mass ratio in Ref. [29] (see also Ref. [24]) to be

$$A(\alpha) = \frac{2\sqrt{2}}{\pi} \frac{1}{1-\alpha} \left[1 - \frac{2\alpha^2}{1+\alpha} \sqrt{\frac{\alpha+1}{\alpha-1}} \arctan \sqrt{\frac{\alpha-1}{\alpha+1}} \right], \quad (\text{B4})$$

with the definition $\sqrt{-1} = i$. The function A is well-defined for equal masses, where

$$A(1) = \frac{8\sqrt{2}}{3\pi}, \quad (\text{B5})$$

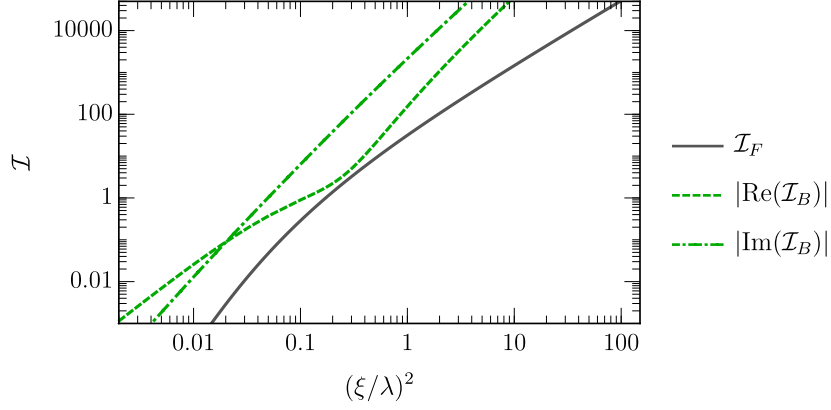


FIG. 4: The functions \mathcal{I}_F (solid, black) and the real (green, dashed) and imaginary (green, dot-dashed) parts of \mathcal{I}_B , calculated for equal masses $m_B = m$. The latter two are negative, therefore we take the absolute values of these.

which leads to $\Sigma_2^F(0) = 32\sqrt{2}a^2n_0/(3m\xi_0)$.

Similarly to the Fröhlich diagrams, we evaluate the “bubble” contribution. We note that again there is a contribution which is present even at $T = 0$. Specifically, this is the term which does not contain a Bose distribution in any of the momentum summations. This term, however, arises from bosons excited out of the condensate (see Fig. 1), and is thus suppressed by a factor $\sqrt{n_0a_B^3}$ compared with the Fröhlich diagrams. This suppression only increases at finite temperature and therefore we ignore this term in the following. Instead, using Eq. (5) we define

$$\begin{aligned}
\tilde{\Sigma}_2^B(T) &= \mathcal{T}_v^2 \sum_{\mathbf{k}} \left\{ f_{\mathbf{k}} [v_{\mathbf{k}}^2 \Pi_{11}(\mathbf{k}, -E_{\mathbf{k}}) + u_{\mathbf{k}}^2 \Pi_{11}(\mathbf{k}, E_{\mathbf{k}}) - u_{\mathbf{k}} v_{\mathbf{k}} \Pi_{12}(\mathbf{k}, E_{\mathbf{k}}) - u_{\mathbf{k}} v_{\mathbf{k}} \Pi_{12}(\mathbf{k}, -E_{\mathbf{k}})] \right. \\
&\quad \left. + v_{\mathbf{k}}^2 \tilde{\Pi}_{11}(\mathbf{k}, -E_{\mathbf{k}}) - u_{\mathbf{k}} v_{\mathbf{k}} \tilde{\Pi}_{12}(\mathbf{k}, -E_{\mathbf{k}}) \right\} \\
&= \Sigma_2^F(T=0) \sqrt{n_0(0)a_B^3} \left(\frac{n_0(T)}{n_0(0)} \right)^2 \frac{(1+1/\alpha)(8\pi)^{5/2}}{2A(\alpha)} \\
&\quad \times \int \frac{d^3k d^3p}{(2\pi)^6} \left\{ -\bar{f}_{\mathbf{k}} \bar{f}_{\mathbf{p}} \left[\frac{\bar{v}_{\mathbf{k}}^2 \bar{u}_{\mathbf{p}}^2 + \bar{u}_{\mathbf{k}} \bar{v}_{\mathbf{k}} \bar{u}_{\mathbf{p}} \bar{v}_{\mathbf{p}}}{\bar{E}_{\mathbf{k}} + \bar{E}_{\mathbf{p}} + \bar{\epsilon}_{\mathbf{k}+\mathbf{p}}} + \frac{\bar{v}_{\mathbf{k}}^2 \bar{v}_{\mathbf{p}}^2 + \bar{u}_{\mathbf{k}}^2 \bar{u}_{\mathbf{p}}^2 + 2\bar{u}_{\mathbf{k}} \bar{v}_{\mathbf{k}} \bar{u}_{\mathbf{p}} \bar{v}_{\mathbf{p}}}{-\bar{E}_{\mathbf{k}} + \bar{E}_{\mathbf{p}} + \bar{\epsilon}_{\mathbf{k}+\mathbf{p}}} + \frac{\bar{u}_{\mathbf{k}}^2 \bar{v}_{\mathbf{p}}^2 + \bar{u}_{\mathbf{k}} \bar{v}_{\mathbf{k}} \bar{u}_{\mathbf{p}} \bar{v}_{\mathbf{p}}}{-\bar{E}_{\mathbf{k}} - \bar{E}_{\mathbf{p}} + \bar{\epsilon}_{\mathbf{k}+\mathbf{p}}} \right] \right. \\
&\quad \left. - \bar{f}_{\mathbf{k}} \left[\frac{\bar{u}_{\mathbf{k}}^2 \bar{v}_{\mathbf{p}}^2 + \bar{v}_{\mathbf{k}}^2 \bar{u}_{\mathbf{p}}^2 + 2\bar{u}_{\mathbf{k}} \bar{v}_{\mathbf{k}} \bar{u}_{\mathbf{p}} \bar{v}_{\mathbf{p}}}{\bar{E}_{\mathbf{k}} + \bar{E}_{\mathbf{p}} + \bar{\epsilon}_{\mathbf{k}+\mathbf{p}}} + \frac{\bar{v}_{\mathbf{k}}^2 \bar{v}_{\mathbf{p}}^2 + \bar{u}_{\mathbf{k}}^2 \bar{u}_{\mathbf{p}}^2 + 2\bar{u}_{\mathbf{k}} \bar{v}_{\mathbf{k}} \bar{u}_{\mathbf{p}} \bar{v}_{\mathbf{p}}}{-\bar{E}_{\mathbf{k}} + \bar{E}_{\mathbf{p}} + \bar{\epsilon}_{\mathbf{k}+\mathbf{p}}} - \frac{\bar{u}_{\mathbf{k}}^2 + \bar{v}_{\mathbf{k}}^2}{(1+\alpha)\bar{\epsilon}_{\mathbf{p}}} \right] \right\} \\
&\equiv \Sigma_2^F(T=0) \sqrt{n_0(0)a_B^3} \left(\frac{n_0(T)}{n_0(0)} \right)^2 \mathcal{I}_B(\xi/\lambda, \alpha). \tag{B6}
\end{aligned}$$

Here, we made the integral in the first line dimensionless by extracting a factor $2m_B/\xi^4$, and defining the dimensionless functions $\bar{E}_{\mathbf{k}} = k\sqrt{2+k^2}$, $\bar{\epsilon}_{\mathbf{k}} = k^2/\alpha$, $\bar{u}_{\mathbf{k}} = \sqrt{\frac{k^2+1}{2E_{\mathbf{k}}} + \frac{1}{2}}$ and $\bar{v}_{\mathbf{k}} = \sqrt{\frac{k^2+1}{2E_{\mathbf{k}}} - \frac{1}{2}}$. $\tilde{\Pi}_{ij}$ refers to the pair propagator including only those terms involving the Bose distribution function $f_{\mathbf{k}}$, as we ignore the term which is suppressed at zero temperature (see discussion in the main text). Comparing Eq. (B6) with Eq. (B1) explicitly shows that it is suppressed by a factor $(n_0a_B^3)^{1/2}$.

The bubble diagrams contain several simple poles, which we treat numerically by introducing a small imaginary part, i.e., by taking $z \rightarrow z + i\delta$ (in the above, this can be achieved by shifting $\bar{\epsilon}_{\mathbf{k}}$ slightly below the real axis), and then extrapolating our results to $\delta = 0$. We estimate the relative error in the evaluation of the bubble diagrams resulting from this procedure to remain well below 1% for all ξ/λ considered.

In Fig. 4 we show the result for the dimensionless functions \mathcal{I}_F and \mathcal{I}_B for equal masses. In this case, the Fröhlich diagrams are purely real, and we see that they are larger than the bubble diagrams except at very small (outside the range shown) or large temperature.

For unequal masses, the main qualitative difference is that the Fröhlich diagram develops a simple pole when $m_B > m$. This is easily integrated over, and in Fig. 5 we show the resulting functions for the particular case of a ^{40}K atom immersed in a ^{87}Rb condensate.

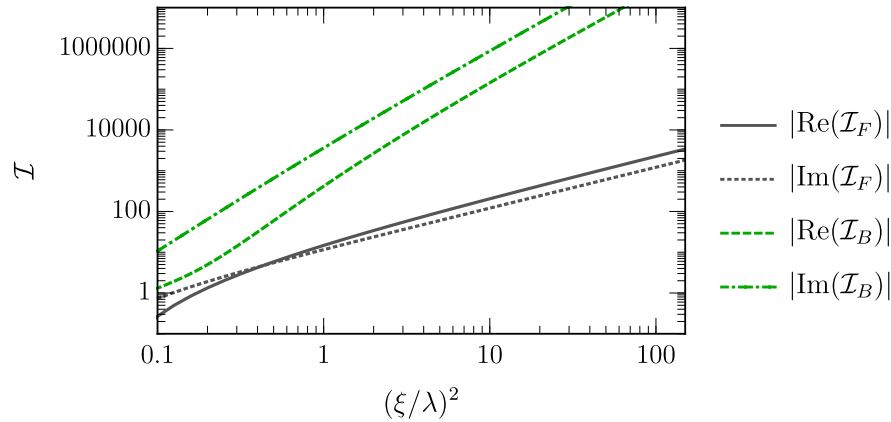


FIG. 5: The dimensionless integrals for a ^{40}K impurity immersed in a ^{87}Rb BEC. We show the real (black, solid) and imaginary (black, dotted) parts of \mathcal{I}_F together with the real (green, dashed) and imaginary (green, dot-dashed) parts of \mathcal{I}_B . These are all negative within the range shown.

Appendix C: Imaginary part of the Fröhlich self-energy

The imaginary part of the Fröhlich self-energy for zero momentum and frequency is found from Eq. (4) of the main text to be

$$\text{Im}\Sigma_2^F(T) = -n_0(T)\mathcal{T}_v^2 \sum_{\mathbf{k}} \frac{\epsilon_{\mathbf{k}}^B}{E_{\mathbf{k}}} f_{\mathbf{k}} \delta(\epsilon_{\mathbf{k}} - E_{\mathbf{k}}). \quad (\text{C1})$$

It follows that the imaginary part is non-zero only if $\epsilon_{\mathbf{k}} = E_{\mathbf{k}}$ has a solution, i.e. if $m < m_B$. Doing the integral (C1) yields

$$\text{Im}\Sigma_2^F(T) = -\frac{2}{\pi} \frac{\alpha^3}{(1-\alpha^2)^{3/2}} \mathcal{T}_v^2 n_0(T)^{3/2} m_B^{3/2} \mathcal{T}_B^{1/2} f_{\mathbf{k}_0} \quad (\text{C2})$$

where \mathbf{k}_0 is the \mathbf{k} vector which solves $\epsilon_{\mathbf{k}} = E_{\mathbf{k}}$.

Appendix D: Self-energy above T_c

Above T_c , the second order self energy reduces to the term from the bubble diagrams

$$\begin{aligned} \Sigma_2(T > T_c) &= \mathcal{T}_v^2 \sum_{\mathbf{k}} f_{\mathbf{k}} \Pi_{11}(\mathbf{k}, E_{\mathbf{k}}) = \mathcal{T}_v^2 \sum_{\mathbf{k}} f_{\mathbf{k}} \sum_{\mathbf{p}} \left(\frac{1 + f_{\mathbf{p}}}{\epsilon_{\mathbf{k}}^B - \epsilon_{\mathbf{p}}^B - \epsilon_{\mathbf{k}-\mathbf{p}} + i0} + \frac{1}{\epsilon_{\mathbf{p}}^B + \epsilon_{\mathbf{k}}} \right) \\ &= \mathcal{T}_v^2 8m_B^2 m_r T^2 \sum_{\mathbf{k}} \frac{1}{e^{k^2/z_{\text{id}}} - 1} \sum_{\mathbf{p}} \left[\left(\frac{1}{p^2} - \frac{1}{p^2 - k^2/\gamma^2 - i0} \right) + \frac{1}{e^{(\mathbf{p}+\mathbf{k}/(1+\alpha))^2/z_{\text{id}}} - 1} \frac{1}{k^2/\gamma^2 - p^2 + i0} \right], \end{aligned} \quad (\text{D1})$$

where in the second line we shifted $\mathbf{p} \rightarrow \mathbf{p} + \mathbf{k}/(1+\alpha)$ in all terms except the renormalization (last term of the first line). We also measured momenta in units of $\sqrt{2m_B T}$ and defined the ratio $m_B/m_r \equiv \gamma$. The quantity $z_{\text{id}} \equiv e^{\mu_{\text{id}}/T}$ is the fugacity of the ideal Bose gas. It is related to the density through

$$n\lambda^3 = \lambda^3 \sum_{\mathbf{k}} f_{\mathbf{k}} = \text{Li}_{3/2}(z_{\text{id}}), \quad (\text{D2})$$

and can be further related to T/T_c through the ideal gas expression

$$T/T_c = [\zeta(3/2)]^{2/3} (n\lambda^3)^{-2/3}. \quad (\text{D3})$$

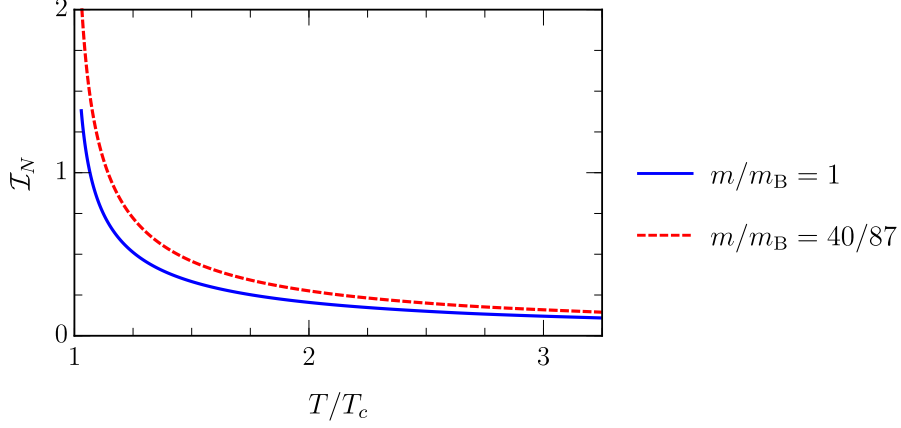


FIG. 6: The dimensionless integral appearing in the self-energy for temperatures above T_c . We show the result both for equal masses (blue, solid), and for a ^{40}K impurity immersed in a ^{87}Rb BEC (red, dashed).

To proceed, we note that the integral over the angle between \mathbf{k} and \mathbf{p} in Eq. (D1) can be performed analytically:

$$\int_{-1}^1 dx \frac{1}{e^{a+bx} - 1} = \frac{1}{b} \log \frac{e^a - e^{-b}}{e^a - e^b}, \quad (\text{D4})$$

assuming $a > b > 0$. Since the integral over the term in parenthesis in the second line of Eq. (D1) is purely imaginary, we have

$$\begin{aligned} \frac{\text{Re}[\Sigma_2(T > T_c)]}{\Sigma_2^F(T=0)} &= \frac{\mathcal{T}_v^2 4m_B^2 m T^2}{\Sigma_2^F(T=0)} \frac{1}{8\pi^4} \int_0^\infty \frac{k dk}{e^{k^2 - \mu_b/T} - 1} \int_0^\infty \frac{p dp \mathcal{P}}{k^2/\gamma^2 - p^2} \log \frac{e^{p^2+k^2/(1+\alpha)^2 - \mu_b/T} - e^{-2kp/(1+\alpha)}}{e^{p^2+k^2/(1+\alpha)^2 - \mu_b/T} - e^{2kp/(1+\alpha)}} \\ &= \frac{-1}{\sqrt{n_0(0)^{1/3} a_B}} \underbrace{\sqrt{\frac{2}{\pi^3}} \frac{1+\alpha}{A(\alpha)} \frac{(T/T_c)^2}{\zeta^{4/3}(3/2)} \int_0^\infty \frac{k dk}{e^{k^2 - \mu_b/T} - 1} \int_0^\infty \frac{p dp \mathcal{P}}{p^2 - k^2/\gamma^2} \log \frac{e^{p^2+k^2/(1+\alpha)^2 - \mu_b/T} - e^{-2kp/(1+\alpha)}}{e^{p^2+k^2/(1+\alpha)^2 - \mu_b/T} - e^{2kp/(1+\alpha)}}}_{\mathcal{I}_N(T/T_c, \alpha)}, \end{aligned} \quad (\text{D5})$$

where \mathcal{P} indicates that only the principal part of the integral should be evaluated. The prefactor which scales as $1/\sqrt{a_B}$ arises from the normalization by $\Sigma_2^F(T=0)$. The integral \mathcal{I}_N is evaluated numerically, and the result is shown in Fig. 6. The function referenced in the main text Eq. (13) is $\mathcal{I}_N(T/T_c) \equiv \mathcal{I}_N(T/T_c, 1)$.

For equal masses, the imaginary part of the self-energy can be determined analytically for all $T > T_c$:

$$\frac{\text{Im}[\Sigma_2(T > T_c)]}{\Sigma_2^F(T=0)} = -\frac{3\sqrt{\pi}}{16\zeta^{4/3}(3/2)} \frac{1}{\sqrt{n_0(0)^{1/3} a_B}} \left(\frac{T}{T_c}\right)^2 \left[\text{Li}_2(z) + \frac{1}{2} \log^2(1-z) \right] \quad (\text{D6})$$

For a ^{40}K impurity in a ^{87}Rb condensate, we evaluate the imaginary part of the self energy numerically, again using Eq. (D4).

1. Logarithmic divergence of Σ_2^B above T_c

For concreteness, we focus on equal masses. One can rewrite the integral appearing in Eq. (D5) at T_c as:

$$\sum_{\mathbf{k}, \mathbf{p}} \frac{f_{\mathbf{k}} f_{\mathbf{p}}}{\epsilon_{\mathbf{k}} - \epsilon_{\mathbf{p}} - \epsilon_{\mathbf{k}-\mathbf{p}} + i0} = -\frac{2T^2 m^3}{(2\pi)^4} \int dp \int dk \frac{pk}{(e^{k^2/2} - 1)(e^{p^2/2} - 1)} \log \left[\frac{p+k-i0}{p-k-i0} \right] \quad (\text{D7})$$

$$\simeq \frac{T^2 m^3}{\pi^4} \int dr \frac{1}{r} \int d\phi \frac{1}{\sin \phi \cos \phi} \log \left[\frac{\cos \phi + \sin \phi - i0}{\cos \phi - \sin \phi - i0} \right] \quad (\text{D8})$$

$$\rightarrow -(19.71 - 21.78i) \frac{T^2 m^3}{\pi^4} \log(r). \quad (\text{D9})$$

Here we have made the transformation $p = r \cos \phi$, $k = r \sin \phi$, and then considered the regime $r \ll 1$. Thus, we see that this integral diverges logarithmically as $r \rightarrow 0$.

-
- [1] C. Chin, R. Grimm, P. Julienne, and E. Tiesinga, *Feshbach resonances in ultracold gases*, *Rev. Mod. Phys.* **82**, 1225 (2010).
- [2] A. Schirotzek, C.-H. Wu, A. Sommer, and M. W. Zwierlein, *Observation of Fermi Polarons in a Tunable Fermi Liquid of Ultracold Atoms*, *Phys. Rev. Lett.* **102**, 230402 (2009).
- [3] C. Kohstall, M. Zaccanti, M. Jag, A. Trenkwalder, P. Massignan, G. M. Bruun, F. Schreck, and R. Grimm, *Metastability and coherence of repulsive polarons in a strongly interacting Fermi mixture*, *Nature (London)* **485**, 615 (2012).
- [4] M. Koschorreck, D. Pertot, E. Vogt, B. Fröhlich, M. Feld, and M. Köhl, *Attractive and repulsive Fermi polarons in two dimensions*, *Nature (London)* **485**, 619 (2012).
- [5] N. B. Jørgensen, L. Wacker, K. T. Skalmstang, M. M. Parish, J. Levinsen, R. S. Christensen, G. M. Bruun, and J. J. Arlt, *Observation of Attractive and Repulsive Polarons in a Bose-Einstein Condensate*, *Phys. Rev. Lett.* **117**, 055302 (2016).
- [6] M.-G. Hu, M. J. Van de Graaff, D. Kedar, J. P. Corson, E. A. Cornell, and D. S. Jin, *Bose Polarons in the Strongly Interacting Regime*, *Phys. Rev. Lett.* **117**, 055301 (2016).
- [7] F. Chevy, *Universal phase diagram of a strongly interacting Fermi gas with unbalanced spin populations*, *Phys. Rev. A* **74**, 063628 (2006).
- [8] N. Prokof'ev and B. Svistunov, *Fermi-polaron problem: Diagrammatic Monte Carlo method for divergent sign-alternating series*, *Phys. Rev. B* **77**, 020408 (2008).
- [9] C. Mora and F. Chevy, *Ground state of a tightly bound composite dimer immersed in a Fermi sea*, *Phys. Rev. A* **80**, 033607 (2009).
- [10] M. Punk, P. T. Dumitrescu, and W. Zwerger, *Polaron-to-molecule transition in a strongly imbalanced Fermi gas*, *Phys. Rev. A* **80**, 053605 (2009).
- [11] R. Combescot, S. Giraud, and X. Leyronas, *Analytical theory of the dressed bound state in highly polarized Fermi gases*, *EPL (Europhysics Letters)* **88**, 60007 (2009).
- [12] X. Cui and H. Zhai, *Stability of a fully magnetized ferromagnetic state in repulsively interacting ultracold Fermi gases*, *Phys. Rev. A* **81**, 041602 (2010).
- [13] P. Massignan and G. M. Bruun, *Repulsive polarons and itinerant ferromagnetism in strongly polarized Fermi gases*, *European Physical Journal D* **65**, 83 (2011), arXiv:1102.0121.
- [14] P. Massignan, M. Zaccanti, and G. M. Bruun, *Polarons, dressed molecules and itinerant ferromagnetism in ultracold Fermi gases*, *Reports on Progress in Physics* **77**, 034401 (2014).
- [15] W. Yi and X. Cui, *Polarons in ultracold Fermi superfluids*, *Phys. Rev. A* **92**, 013620 (2015).
- [16] S. P. Rath and R. Schmidt, *Field-theoretical study of the Bose polaron*, *Phys. Rev. A* **88**, 053632 (2013).
- [17] J. Levinsen, M. M. Parish, and G. M. Bruun, *Impurity in a Bose-Einstein Condensate and the Efimov Effect*, *Phys. Rev. Lett.* **115**, 125302 (2015).
- [18] Y. E. Shchadilova, R. Schmidt, F. Grusdt, and E. Demler, *Quantum Dynamics of Ultracold Bose Polarons*, *Phys. Rev. Lett.* **117**, 113002 (2016).
- [19] F. Grusdt, R. Schmidt, Y. E. Shchadilova, and E. A. Demler, *Strong coupling Bose polarons in a BEC*, ArXiv e-prints (2017), arXiv:1704.02605 [cond-mat.quant-gas].
- [20] A. Boudjemâa, *Self-localized state and solitons in a Bose-Einstein-condensate impurity mixture at finite temperature*, *Phys. Rev. A* **90**, 013628 (2014).
- [21] R. Schmidt, H. R. Sadeghpour, and E. Demler, *Mesoscopic Rydberg Impurity in an Atomic Quantum Gas*, *Phys. Rev. Lett.* **116**, 105302 (2016).
- [22] N.-E. Guenther, P. Massignan, M. Lewenstein, and G. M. Bruun, *Bose polarons at finite temperature and strong coupling*, ArXiv e-prints (2017), arXiv:1708.08861 [cond-mat.quant-gas].
- [23] H. Shi and A. Griffin, *Finite-temperature excitations in a dilute Bose-condensed gas*, *Physics Reports* **304**, 1 (1998).
- [24] R. S. Christensen, J. Levinsen, and G. M. Bruun, *Quasiparticle Properties of a Mobile Impurity in a Bose-Einstein Condensate*, *Phys. Rev. Lett.* **115**, 160401 (2015).
- [25] T. T. Wu, *Ground State of a Bose System of Hard Spheres*, *Phys. Rev.* **115**, 1390 (1959).
- [26] K. Sawada, *Ground-State Energy of Bose-Einstein Gas with Repulsive Interaction*, *Phys. Rev.* **116**, 1344 (1959).
- [27] B.-B. Huang and S.-L. Wan, *Polaron in Bose-Einstein-Condensation System*, *Chinese Physics Letters* **26**, 080302 (2009).
- [28] A. Novikov and M. Ovchinnikov, *A diagrammatic calculation of the energy spectrum of quantum impurity in degenerate Bose-Einstein condensate*, *Journal of Physics A: Mathematical and Theoretical* **42**, 135301 (2009).
- [29] W. Casteels and M. Wouters, *Polaron formation in the vicinity of a narrow Feshbach resonance*, *Phys. Rev. A* **90**, 043602 (2014).
- [30] A. E. Glassgold, A. N. Kaufman, and K. M. Watson, *Statistical Mechanics for the Nonideal Bose Gas*, *Phys. Rev.* **120**, 660 (1960).
- [31] I. Khalatnikov, *An Introduction to the Theory of Superfluidity*, Advanced Books Classics Series (Avalon Publishing, New York, 2000).
- [32] J. O. Andersen, *Theory of the weakly interacting Bose gas*, *Rev. Mod. Phys.* **76**, 599 (2004).
- [33] G. Baym and C. Pethick, *Landau Fermi-Liquid Theory: Concepts and Applications* (Wiley-VCH, 1991).
- [34] E. Dagotto, *Correlated electrons in high-temperature superconductors*, *Rev. Mod. Phys.* **66**, 763 (1994).
- [35] A. Kaminski and S. Das Sarma, *Polaron Percolation in Diluted Magnetic Semiconductors*, *Phys. Rev. Lett.* **88**, 247202 (2002).
- [36] R. Bishop, *On the ground state of an impurity in a dilute fermi gas*, *Annals of Physics* **78**, 391 (1973).